International Journal of Solids and Structures 49 (2012) 2187–2194

Contents lists available at SciVerse ScienceDirect

International Journal of Solids and Structures

journal homepage: www.elsevier.com/locate/ijsolstr

A dynamic finite element method for inhomogeneous deformation and electromechanical instability of dielectric elastomer transducers

Harold S. Park [a,*], Zhigang Suo [b], Jinxiong Zhou [c], Patrick A. Klein [d]

[a] Department of Mechanical Engineering, Boston University, Boston, MA 02215, United States
[b] School of Engineering and Applied Sciences, Kavli Institute for Nanobio Science and Technology, Harvard University, Cambridge, MA 02138, United States
[c] MOE Key Laboratory for Strength and Vibration and School of Aerospace, Xi'an Jiaotong University, Xi'an 710049, PR China
[d] Franklin Templeton Investments, San Mateo, CA 94403, United States

ARTICLE INFO

Article history:
Received 20 December 2011
Received in revised form 14 March 2012
Available online 5 May 2012

Keywords:
Dielectric elastomer
Finite element
Electromechanical instability
Wrinkling
Snap through

ABSTRACT

We present a three-dimensional nonlinear finite element formulation for dielectric elastomers. The mechanical and electrical governing equations are solved monolithically using an implicit time integrator, where the governing finite element equations are given for both static and dynamic cases. By accounting for inertial terms in conjunction with the Arruda–Boyce rubber hyperelastic constitutive model, we demonstrate the ability to capture the various modes of inhomogeneous deformation, including pull-in instability and wrinkling, that may result in dielectric elastomers that are subject to various forms of electrostatic loading. The formulation presented here forms the basis for needed computational tools that can elucidate the electromechanical behavior and properties of dielectric elastomers that are used for engineering applications.

1. Introduction

Dielectric elastomers are a class of soft active materials, enabling electromechanical transduction and soft machines (Carpi et al., 2010; Brochu and Pei, 2010; Suo, 2010). When a membrane of a dielectric elastomer is sandwiched between two compliant electrodes and subject to voltage, the membrane reduces thickness and expands area. This phenomenon has led to many designs of transducers with broad applications, including artificial muscles for soft robots and adaptive optics, as well as generators to harvest energy from human walking and ocean waves.

Further development of dielectric elastomer transducers demands accurate and efficient computational methods. The transducers involve nonlinear electromechanical coupling, and are often structures of tensegrity—hybrids of soft membranes in tension and hard materials in compression. Voltage-induced deformation can be very large (Pelrine et al., 2000; Keplinger et al., 2008), typically limited by electromechanical instability (Wissler and Mazza, 2005a; Plante and Dubowsky, 2006; Zhao and Suo, 2007; Norris, 2008; Kollosche and Kofod, 2010). Furthermore, the electromechanical instability can be harnessed to achieve giant voltage-induced deformation (Zhao and Suo, 2010; Koh et al., 2011; Keplinger et al., 2012).

For a computational approach to be broadly useful, finite element method is anticipated. Several papers have appeared on the finite element method for dielectric elastomers (Zhao and Suo, 2008; Vu et al., 2007; Zhou et al., 2008; O'Brien et al., 2009; Wissler and Mazza, 2005b; Wissler and Mazza, 2007). The approaches of Zhao and Suo (2008) and O'Brien et al. (2009) are similar in that neither formulation accounted for the full electromechanical coupling, i.e. electrostatic effects were accounted for via inclusion in the mechanical free energy, while no electrostatic governing equation was solved. The approaches of Vu et al. (2007) and Zhou et al. (2008) are similar in that both utilized finite deformation, fully coupled electromechanical equations that were solved neglecting inertia. While the work of Vu et al. (2007) did not consider electromechanical instabilities, such effects were considered by Zhou et al. (2008), though difficulties in tracking the entire history of the electromechanical instability were found due to the static formulation. Wissler and Mazza (2007) solved the coupled electromechanical problem using Poisson's equation for the electrostatics, though again, electromechanical instabilities were not considered. Overall, it is clear that a key unresolved issue in numerical modeling of dielectric elastomers is the ability to capture inhomogeneous deformation accompanying electromechanical instability.

This paper presents a three-dimensional finite element method for dielectric elastomer transducers. To capture electromechanical instability, we include inertial effects and solve the mechanical and electrical governing equations monolithically. We give the resulting finite element equations, comment on their structure as

* Corresponding author.
E-mail address: parkhs@bu.edu (H.S. Park).

0020-7683/$ - see front matter © 2012 Elsevier Ltd. All rights reserved.
http://dx.doi.org/10.1016/j.ijsolstr.2012.04.031

compared to the quasistatic case, and then present examples of instability and inhomogeneous deformation.

2. Nonlinear field theory of dielectric elastomers

Our finite element method is formulated on the basis a nonlinear electromechanical field theory (Suo et al., 2008); see a recent review of the theory of dielectric elastomers (Suo, 2010). Here we summarize the essential equations.We evolve in time the state of a dielectric elastomer transducer subject to electromechanical loads. Name each material particle of the transducer by its coordinate $\mathbf{X}$ when the transducer is in a reference state. At time t, the material particle moves to a place of coordinate $\mathbf{x}$. The function $\mathbf{x}(\mathbf{X},t)$ describes the deformation of the transducer in time. Define the deformation gradient by

$$F_{iJ}=\frac{\partial x_i(\mathbf{X},t)}{\partial X_J} \tag{1}$$

Let $\Phi(\mathbf{X},t)$ be the electric potential of material particle $\mathbf{X}$ and time t. Define the nominal electric field by

$$\tilde{E}_I=-\frac{\partial \Phi(\mathbf{X},t)}{\partial X_I} \tag{2}$$

The nominal stress s_{iJ} satisfies the statement of virtual work:

$$\int s_{iJ}\frac{\partial \xi_i}{\partial X_J}dV=\int\left(B_i-\rho\frac{\partial^2 x_i}{\partial t^2}\right)\xi_i dV+\int T_i\xi_i dA \tag{3}$$

where $\xi_i(\mathbf{X})$ is an arbitrary vector function, B_i the body force, ρ the mass density, and T_i the traction. The nominal electric displacement $\tilde{D}_I$ satisfies the statement of virtual work:

$$-\int \tilde{D}_I\frac{\partial \eta}{\partial X_I}dV=\int q\eta dV+\int \omega\eta dA \tag{4}$$

where $\eta(\mathbf{X})$ is an arbitrary scalar test function, q the volumetric charge density, and ω the surface charge density. In (3) and (4), the integrals are carried out over material particles—that is, over volume and surface in the reference state of the transducer. The mechanical equation (3) includes inertia, while the electrical equation (4) is electrostatic. Essential boundary conditions can be applied via the displacement and electric potential, while natural boundary conditions can be applied via traction and electric charges.

To focus on main ideas, we will not be concerned with any thermal effects. The thermodynamics of the dielectric elastomer is specified by a free-energy function $\hat{W}$. Associated with small changes $\delta\mathbf{F}$ and $\delta\tilde{\mathbf{E}}$, the free energy changes by

$$\delta\hat{W}=s_{iJ}\delta F_{iJ}-\tilde{D}_J\delta\tilde{E}_J \tag{5}$$

To ensure that the free energy is invariant with respect to rigid-body rotation, the free energy depends on the deformation gradient through the tensor $C_{IJ}=F_{kI}F_{kJ}$. Consequently, (5) implies that

$$\begin{aligned} s_{iJ}&=2F_{iL}\frac{\partial\hat{W}(\mathbf{C},\tilde{\mathbf{E}})}{\partial C_{JL}},\\ \tilde{D}_J&=-\frac{\partial\hat{W}(\mathbf{C},\tilde{\mathbf{E}})}{\partial\tilde{E}_J}\end{aligned} \tag{6}$$

Once the function $\hat{W}(\mathbf{C},\tilde{\mathbf{E}})$ is specified for a dielectric elastomer, (6) gives the equations of state.

At a given state $(\mathbf{F},\tilde{\mathbf{E}})$, (6) can be linearized as

$$\begin{aligned} \Delta s_{iJ}&=H_{iJkL}\Delta F_{kL}-e_{iJL}\Delta\tilde{E}_L,\\ \Delta\tilde{D}_J&=e_{iJL}\Delta F_{iL}+\varepsilon_{JL}\Delta\tilde{E}_L\end{aligned} \tag{7}$$

where the tangent moduli are (Zhou et al., 2008)

$$\begin{aligned} H_{iJkL}&=2\delta_{ik}\frac{\partial\hat{W}(\mathbf{C},\tilde{\mathbf{E}})}{\partial C_{JL}}+4F_{iM}F_{kN}\frac{\partial^2\hat{W}(\mathbf{C},\tilde{\mathbf{E}})}{\partial C_{JM}\partial C_{LN}},\\ e_{iJL}&=-2F_{iM}\frac{\partial^2\hat{W}(\mathbf{C},\tilde{\mathbf{E}})}{\partial C_{JM}\partial\tilde{E}_L},\\ \varepsilon_{JL}&=-\frac{\partial^2\hat{W}(\mathbf{C},\tilde{\mathbf{E}})}{\partial\tilde{E}_J\partial\tilde{E}_L}\end{aligned} \tag{8}$$

3. Finite-element discretization

We adopt the standard finite-element discretization for both the displacement field and the electric potential:

$$\begin{aligned} \mathbf{x}(\mathbf{X},t)-\mathbf{X}&=\sum N_a(\mathbf{X})\mathbf{u}_a(t),\\ \Phi(\mathbf{X},t)&=\sum N_a(\mathbf{X})\Phi_a(t)\end{aligned} \tag{9}$$

where $N_a(\mathbf{X})$ are shape functions, $\mathbf{u}_a(t)$ is the nodal displacement and $\Phi_a(t)$ is the nodal electric potential; the sum is taken over all nodes. We adopt the same discretization for the test functions:

$$\begin{aligned} \xi_i(\mathbf{X})&=\sum N_a(\mathbf{X})\xi_{ia},\\ \eta(\mathbf{X})&=\sum N_a(\mathbf{X})\eta_a\end{aligned} \tag{10}$$

This Bubnov–Galerkin approximation converts (3) and (4) into the discretized form:

$$\int s_{iJ}\frac{\partial N_a}{\partial X_J}dV=\int B_iN_adV+\int T_iN_adA-\sum\ddot{u}_{ib}\int\rho N_bN_adV \tag{11}$$

$$-\int\tilde{D}_I\frac{\partial N_a}{\partial X_I}dV=\int qN_adV+\int\omega N_adA \tag{12}$$

Denote the column of nodal values of displacement by $\mathbf{u}$, that of velocity by $\mathbf{v}$, that of acceleration by $\mathbf{a}$, and that of electric potential by Φ. Eq. (11) is a nonlinear ordinary differential equation, which relates nodal values of acceleration to a nonlinear function of the nodal values of displacement and electric potential:

$$\mathbf{g}(\mathbf{u},\Phi,t)=\mathbf{Ma} \tag{13}$$

The matrix $\mathbf{M}$ has elements of the form $\int\rho N_bN_adV$. Eq. (12) is a nonlinear algebraic equation of the nodal values of displacement and electric potential:

$$\mathbf{h}(\mathbf{u},\Phi,t)=0 \tag{14}$$

The coupled ordinary differential equation (13) and algebraic equation (14) evolve the two columns $(\mathbf{u}(t))$ and $\Phi(t)$.

3.1. Quasistatic formulation

In the quasistatic formulation (i.e. neglecting inertia), (11) becomes a nonlinear algebraic equation of the nodal values of displacement and electric potential. The simultaneous nonlinear algebraic equations (11) and (12) may be solved by using the Newton–Raphson method (Vu et al., 2007; Zhou et al., 2008). In the incremental form, (11) and (12) becomes

$$\begin{bmatrix}\mathbf{K}_{mm} & \mathbf{K}_{me}\\ \mathbf{K}_{me}^T & \mathbf{K}_{ee}\end{bmatrix}\begin{bmatrix}\Delta\mathbf{u}\\ \Delta\Phi\end{bmatrix}=\begin{bmatrix}\mathbf{f}_m\\ \mathbf{f}_e\end{bmatrix} \tag{15}$$

The matrices $\mathbf{K}_{mm}$, $\mathbf{K}_{me}$, and $\mathbf{K}_{ee}$ have elements of the forms, respectively,

$$\int H_{iJkL}\frac{\partial N_a}{\partial X_J}\frac{\partial N_b}{\partial X_L}dV,-\int_V e_{kJL}\frac{\partial N_a}{\partial X_J}\frac{\partial N_b}{\partial X_L}dV,-\int_V\varepsilon_{JL}\frac{\partial N_a}{\partial X_J}\frac{\partial N_b}{\partial X_L}dV \tag{16}$$

The columns $\mathbf{f}_m$ and $\mathbf{f}_e$ have elements of the forms, respectively,

$$\int_V B_i N_a dV + \int_A T_i N_a dA - \int_V s_{ij} \frac{\partial N_a}{\partial X_J} dV,$$
$$\int_V q N_a dV + \int_A \omega N_a dA + \int_V \tilde{D}_J \frac{\partial N_a}{\partial X_J} dV \tag{17}$$

The Newton–Raphson method breaks down when the Hessian in (15) is singular. The singular Hessian also corresponds to the condition of electromechanical instability (Zhao and Suo, 2007).

3.2. Dynamic formulation

If inertial effects are considered, the governing equations are different in structure from those of Vu et al. (2007) and Zhou et al. (2008), who did not consider inertial effects. We use inertia to capture physical details that may arise during the electromechanical softening and instability of the dielectric elastomer. Furthermore, the simple nature of including inertial effects to capture the electromechanical instability stands in contrast to the complex arc-length (Belytschko et al., 2002) or continuation-type methods that can also be utilized to capture the post-instability response for materials.

Let t^n and t^{n+1} be two consecutive discrete times, and let $\Delta t = t^{n+1} - t^n$ be the time step. Write $\mathbf{u}^n = \mathbf{u}(t^n)$ and $\mathbf{u}^{n+1} = \mathbf{u}(t^{n+1})$, etc. We use the Newmark implicit dynamic integrator (Belytschko et al., 2002; Hughes, 1987):

$$\mathbf{u}^{n+1} = \mathbf{u}^n + \Delta t \mathbf{v}^n + \Delta t^2 \left(\frac{1}{2} - \beta\right)\mathbf{a}^n + \beta \Delta t^2 \mathbf{a}^{n+1},$$
$$\mathbf{v}^{n+1} = \mathbf{v}^n + \Delta t(1-\gamma)\mathbf{a}^n + \gamma \Delta t \mathbf{a}^{n+1} \tag{18}$$

The integrator is unconditionally stable if the parameters are set to $\beta = 1/4$ and $\gamma = 1/2$.

At time t^{n+1}, the coupled ordinary differential equation (13) and algebraic equation (14) become

$$\mathbf{g}(\mathbf{u}^{n+1}, \Phi^{n+1}, t^{n+1}) = \frac{\mathbf{M}}{\beta \Delta t^2}\left[\mathbf{u}^{n+1} - \mathbf{u}^n - \Delta t \mathbf{v}^n - \Delta t^2 \left(\frac{1}{2} - \beta\right)\mathbf{a}^n\right] \tag{19}$$

$$\mathbf{h}(\mathbf{u}^{n+1}, \Phi^{n+1}, t^{n+1}) = 0 \tag{20}$$

In deriving (19), we have combined (13) and (18). Eqs. (19) and (20) are coupled nonlinear algebraic equations for $(\mathbf{u}^{n+1}, \Phi^{n+1})$. We solve for $(\mathbf{u}^{n+1}, \Phi^{n+1})$ by using the Newton–Raphson method. The iterative equation takes the form

$$\begin{bmatrix} \mathbf{K}_{mm} + \frac{1}{\beta \Delta t^2}\mathbf{M} & \mathbf{K}_{me} \\ \mathbf{K}_{me}^T & \mathbf{K}_{ee} \end{bmatrix} \begin{bmatrix} \Delta \mathbf{u}^{n+1} \\ \Delta \Phi^{n+1} \end{bmatrix} = \begin{bmatrix} \mathbf{f}_m + \frac{\mathbf{M}}{\beta \Delta t^2}\left[\mathbf{u}^n + \Delta t \mathbf{v}^n + \Delta t^2 (\frac{1}{2} - \beta)\mathbf{a}^n - \mathbf{u}^{n+1}\right] \\ \mathbf{f}_e \end{bmatrix} \tag{21}$$

This is a nonlinear algebraic equation for $(\Delta \mathbf{u}^{n+1}, \Delta \Phi^{n+1})$. The equation is solved repeatedly to improve the root of $(\mathbf{u}^{n+1}, \Phi^{n+1})$. At each iteration, the current values of $(\mathbf{u}^{n+1}, \Phi^{n+1})$ are used to evaluate the Hessian and the right-hand side. Observe that the matrix $\mathbf{M}$ is positive-definite. When the time step Δt is sufficiently small, the Hessian will remain nonsingular.

4. Model of ideal dielectric elastomers

An elastomer is a three-dimensional network of long and flexible polymers, held together by crosslinks. Each polymer chain consists of a large number of monomers. Consequently, the crosslinks have negligible effect on the polarization of the monomers—that is, the elastomer can polarize nearly as freely as a polymer melt. As an idealization, we may assume that the dielectric behavior of an elastomer is exactly the same as that of a polymer melt. This model of ideal dielectric elastomers has the free energy of the form (Zhao et al., 2007)

$$\hat{W}(\mathbf{C}, \tilde{\mathbf{E}}) = W_{stretch}(\mathbf{C}) - \frac{\varepsilon}{2} J C_{IJ}^{-1} \tilde{E}_I \tilde{E}_J \tag{22}$$

where $W_{stretch}(\mathbf{C})$ is the free energy of the elastomer in the absence of electric field, ε is the permittivity of the material, $J = \det \mathbf{F}$ is the determinant of the deformation gradient.

In an elastomer, each individual polymer chain has a finite contour length. When the elastomer is subject no loads, the polymer chains are coiled, allowing a large number of conformations. Subject to loads, the polymer chains become less coiled. As the loads increase, the end-to-end distance of each polymer chain approaches the finite contour length, and the elastomer approaches a limiting stretch. On approaching the limiting stretch, the elastomer stiffens steeply. This effect is absent in the neo-Hookean model, but is represented by Arruda and Boyce (1993) model:

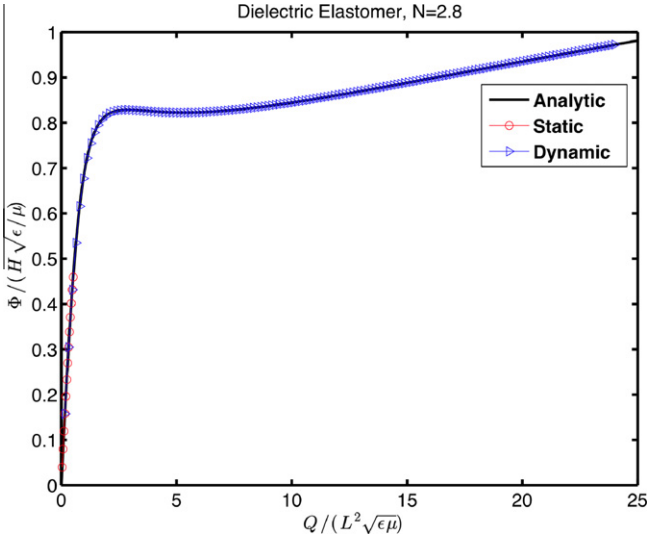

Fig. 1. Deformation of a dielectric elastomer subject to applied charge loading for $N = 2.8$ as obtained using static and dynamic FEM formulations.

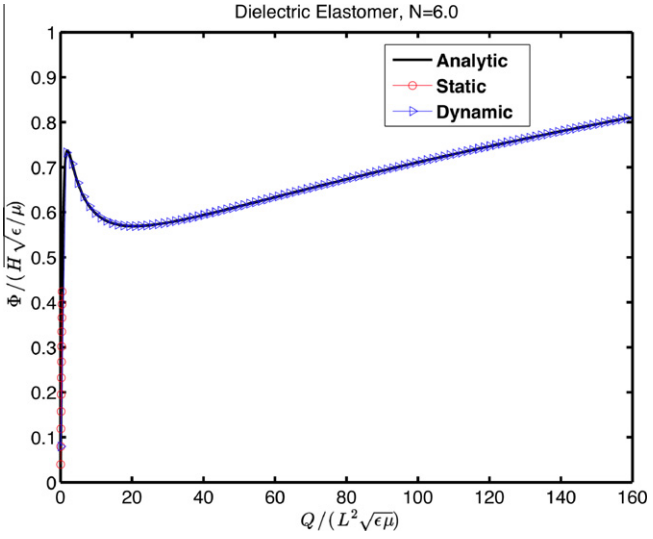

Fig. 2. Deformation of a dielectric elastomer subject to applied charge loading for $N = 6$ as obtained using static and dynamic FEM formulations.

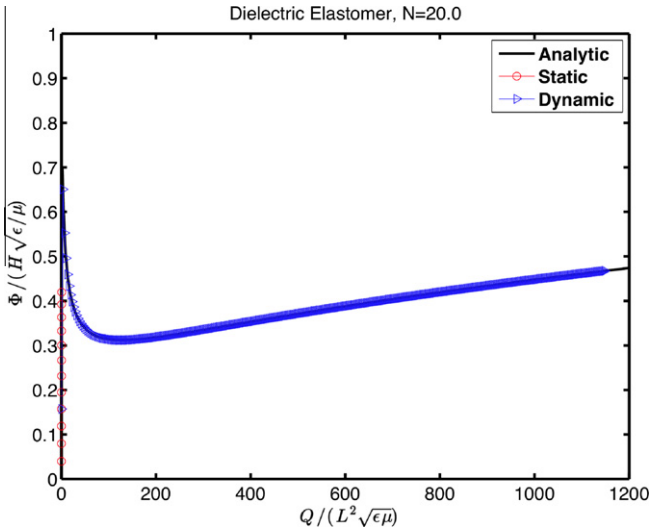

Fig. 3. Deformation of a dielectric elastomer subject to applied charge loading for $N = 20$ as obtained using static and dynamic FEM formulations.

$$\frac{W_{stretch}}{\mu} = \frac{1}{2}(I-3) + \frac{1}{20N}(I^2-9) + \frac{11}{1050N^2}(I^3-27) + \frac{19}{7000N^3}(I^4-81) + \frac{519}{673750N^4}(I^5-243) \tag{23}$$

where μ is the shear modulus, N is the number of links per polymer chain and $I = C_{KK}$. The Arruda–Boyce model reduces to the Neo-Hookean model if $N \to \infty$.

The complete expression for the dielectric elastomer free energy can be written as

$$\hat{W}(\mathbf{C},\tilde{\mathbf{E}}) = W_{stretch}(I) + \frac{1}{2}\lambda(\log J)^2 - 2W'_{stretch}(3)\log J - \frac{\varepsilon}{2}JC^{-1}_{IJ}\tilde{E}_I\tilde{E}_J \tag{24}$$

The incompressibility condition that is required for accurate modeling of dielectric elastomers is enforced approximately through the parameter λ, which represents the bulk modulus; specifically, it is enforced through a penalty-like manner by taking the ratio of λ/μ (or the ratio of the bulk modulus to the shear modulus) to be a large value, typically on the order of 10^4–10^6, where the upper bound value of $\lambda/\mu = 10^6$ is used in the present work to maximize the convergence rate.

The free energy of the ideal dielectric elastomer given in (24) neglects creep and other dissipative effects, in particular viscoelasticity and current leakage. Dissipative effects can easily be included in the free energy, see for example see Hong (2011) and Foo et al. (2012) for dissipative effects. We also note that a comparison between the theory of the ideal dielectric elastomer and experiment was recently made in a simple setting by Huang et al. (2012): a membrane under equi-biaxial dead loads and ramping voltage.

The analytic expressions of the free energy derivatives that are needed for the various stresses and moduli are now given as follows

$$2\frac{\partial\hat{W}(\mathbf{C},\tilde{\mathbf{E}})}{\partial C_{IJ}} = 2W'_{stretch}(I)\delta_{IJ} + (\lambda\log J - 2W'_{stretch}(3))C^{-1}_{IJ} + \varepsilon J\tilde{E}_K\tilde{E}_L\left(C^{-1}_{KI}C^{-1}_{LJ} - \frac{1}{2}C^{-1}_{KL}C^{-1}_{IJ}\right) \tag{25}$$

The nominal electric displacement can be written as

$$\tilde{D}_I = \varepsilon J\tilde{E}_J C^{-1}_{IJ} \tag{26}$$

The tangent moduli that are required for the weak form can be obtained by taking the second derivatives of the free energy function to give

$$\begin{aligned}4\frac{\partial^2 W(\mathbf{C},\tilde{\mathbf{W}})}{\partial C_{IJ}\partial C_{KL}} &= 4W''_{stretch}(I)\delta_{IJ}\delta_{KL} + (2W'_{stretch}(3) - \lambda\ln J)\\ &\times (C^{-1}_{IK}C^{-1}_{JL} + C^{-1}_{IL}C^{-1}_{JK}) + \lambda C^{-1}_{IJ}C^{-1}_{KJ}\\ &+ \varepsilon J\tilde{E}_M\tilde{E}_N\left[\frac{1}{2}C^{-1}_{MN}(C^{-1}_{IK}C^{-1}_{JL} + C^{-1}_{IL}C^{-1}_{JK}) + C^{-1}_{MK}C^{-1}_{NL}C^{-1}_{IJ}\right.\\ &+ \left.\left(C^{-1}_{MI}C^{-1}_{NJ} - \frac{1}{2}C^{-1}_{MN}C^{-1}_{IJ}\right)C^{-1}_{KL}\right]\varepsilon J\tilde{E}_M\tilde{E}_N[C^{-1}_{MI}(C^{-1}_{NK}C^{-1}_{JL}\\ &+ C^{-1}_{NL}C^{-1}_{JK}) + C^{-1}_{NJ}(C^{-1}_{IK}C^{-1}_{ML} + C^{-1}_{IL}C^{-1}_{MK})]\end{aligned} \tag{27}$$

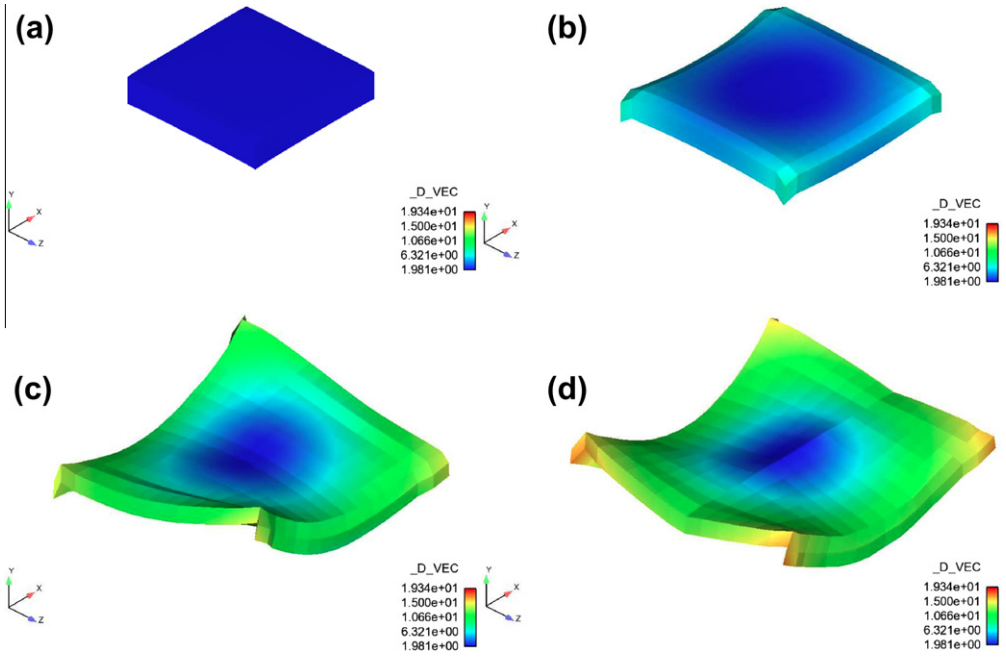

Fig. 4. Time history of deformation of a free-standing 3D dielectric elastomer under charge loading. (a) Undeformed configuration, (b–d) various stages of deformation after the electromechanical instability has occurred.

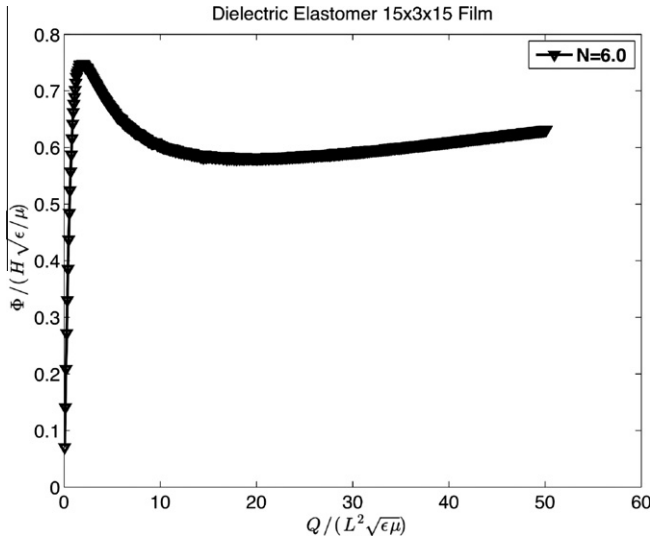

Fig. 5. Voltage vs. charge curve corresponding to the deformation of the free-standing 3D dielectric elastomer thin film subject to charge loading shown in Fig. 4.

$$2\frac{\partial^2 W(\mathbf{C},\tilde{\mathbf{E}})}{\partial C_{JK}\partial \tilde{E}_I} = \varepsilon J \tilde{E}_L (C^{-1}_{KL}C^{-1}_{IJ} - C^{-1}_{KI}C^{-1}_{JL} - C^{-1}_{IL}C^{-1}_{JK}) \tag{28}$$

and

$$\frac{\partial^2 W(\mathbf{C},\tilde{\mathbf{E}})}{\partial \tilde{E}_K \partial \tilde{E}_L} = \varepsilon J C^{-1}_{IJ} \tag{29}$$

5. Numerical results

We embed the above model into the Sandia-developed simulation code Tahoe (2011) using regular meshes of 8-node hexahedral elements. The values for the material constants in the free energy in (26) were $\mu = \varepsilon = 1$ and $\lambda = 1{,}000{,}000$. In all cases where an applied potential boundary condition was applied, it is assumed that the electrodes are sufficiently compliant such that they do not constrain the deformation of the dielectric elastomer film. Furthermore, the initial conditions for the mechanical domain were always set to zero, i.e. the initial displacements and velocities of all nodes were set to zero for all examples considered below.

5.1. Homogeneous deformation: static vs. dynamic comparison

Our first example is the homogeneous deformation of a dielectric elastomer sandwiched between two compliant electrodes. The stability of the homogeneous deformation has been analyzed analytically in Keplinger et al. (2012). The electrostatic boundary conditions were specified such that the voltage was zero at one electrode (on the $-y$ surface), while the charge at the other electrode (the $+y$ surface) was increased monotonically. The dimensions of the dielectric elastomer were $l = w = h = 1$, which was discretized by a single 8-node hexahedral finite element. The purpose of this example is to demonstrate the ability to capture the electromechanical instability through the inclusion of inertial effects.

The results as shown in Figs. 1–3 are similar to those obtained by Zhou et al. (2008) in that as N is increased, the quasistatic calculation fails before the electromechanical instability occurs due to non-convergence of the solution; we note that the onset of the electromechanical instability corresponds to a softening in the voltage-charge curve in Figs. 1–3.

However, if the dynamic formulation is utilized, the large deformation behavior and electromechanical instability is captured for various values of N. In particular, it can be seen that for Figs. 1–3, the dynamic formulation captures not only the initial softening of the voltage vs. charge curve, but then the subsequent stiffening that occurs at large values of applied charge. Because the dynamic problem is time-dependent, the values shown in Figs. 1–3 correspond to the converged values of potential and charge that result

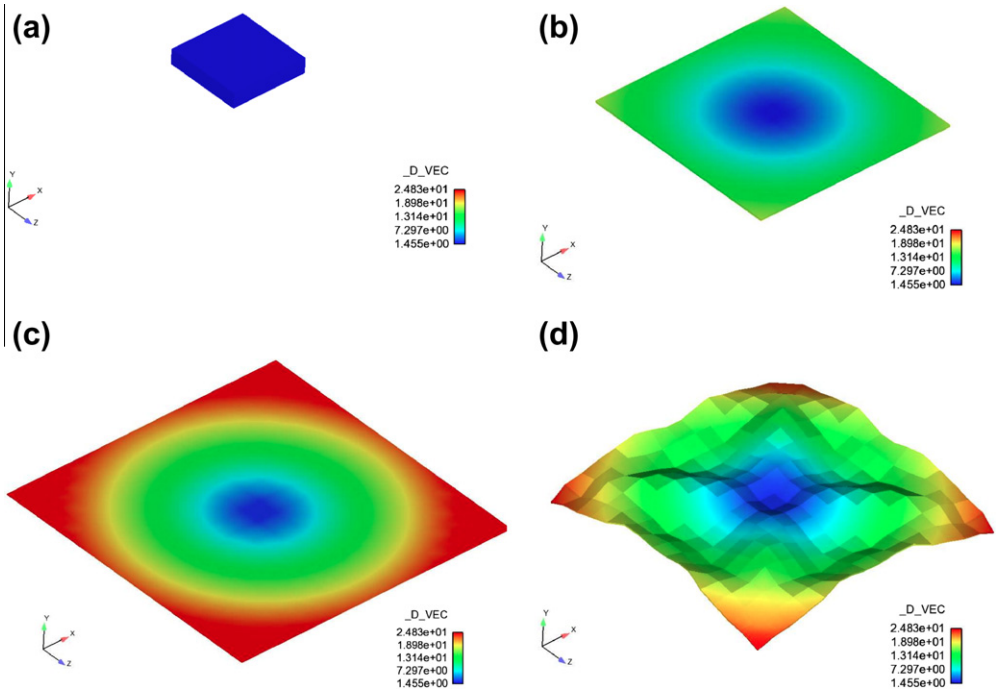

Fig. 6. Time history of deformation leading to pull-in instability and failure of a free-standing 3D dielectric elastomer under potential loading. (a) Undeformed configuration, (b–d) various stages of deformation leading to failure of the dielectric elastomer film.

at each time step. We also plot in Fig. 1–3 the corresponding analytic solution obtained for this problem (Zhao et al., 2007). It is clear that for all values of N, the dynamic FEM formulation captures the homogeneous deformation and electromechanical instability very accurately as compared to the analytic solution.

5.2. Inhomogeneous deformation: freestanding 3D film

We now present three-dimensional examples to demonstrate the capability of the proposed dynamic formulation in capturing electromechanical instabilities in 3D dielectric elastomers. Our first example is that of a free standing film, with dimensions $15 \times 3 \times 15$ in the x, y and z-directions, respectively. 675 8-node hexahedral finite elements with a regular edge length of 1 were utilized to discretize the film. There were no mechanical constraints on the film, while two different electrostatic boundary conditions were used. For the first, the $-y$ surface of the film was kept zero electric potential, while the $+y$ surface of the film was subject to a monotonically increasing value of applied charge. For the second, the $-y$ surface was also kept zero potential, while the $+y$ surface of the film was subject to a monotonically increasing value of potential. The condition of using a potential difference to induce the deformation of the dielectric elastomer is the standard approach that has been utilized experimentally over the past decade; however, Keplinger et al. (2008) recently demonstrated a new experimental technique by which charge, and not potential loading could be used to deform the dielectric elastomer.

Fig. 4 shows the time history of deformation of the elastomer under charge loading. As can be seen going from Fig. 4(a) to (b), the initially undeformed film in Fig. 4(a) undergoes significant contraction in the thickness (y)-direction and expansion in the lateral (x and z)-directions, where the inhomogeneous deformation that occurs due to the softening in the voltage vs. charge curve in Fig. 5 is illustrated in Figs. 4(b)–(d). Specifically, after the peak of the voltage vs. charge curve is passed as shown in Fig. 5, the film begins flexing in different modes, first about the z-axis in Fig. 4(c), and then about both the xy and xz-axes in Fig. 4(d). The dynamic formulation enables the resolution of the time-dependent instability modes as shown in Fig. 4 that may be obscured by analyzing the voltage vs. charge curve alone, as it can be observed that those curves are similar for the film in Fig. 5, and for the single element curve undergoing homogeneous deformation in Fig. 2.

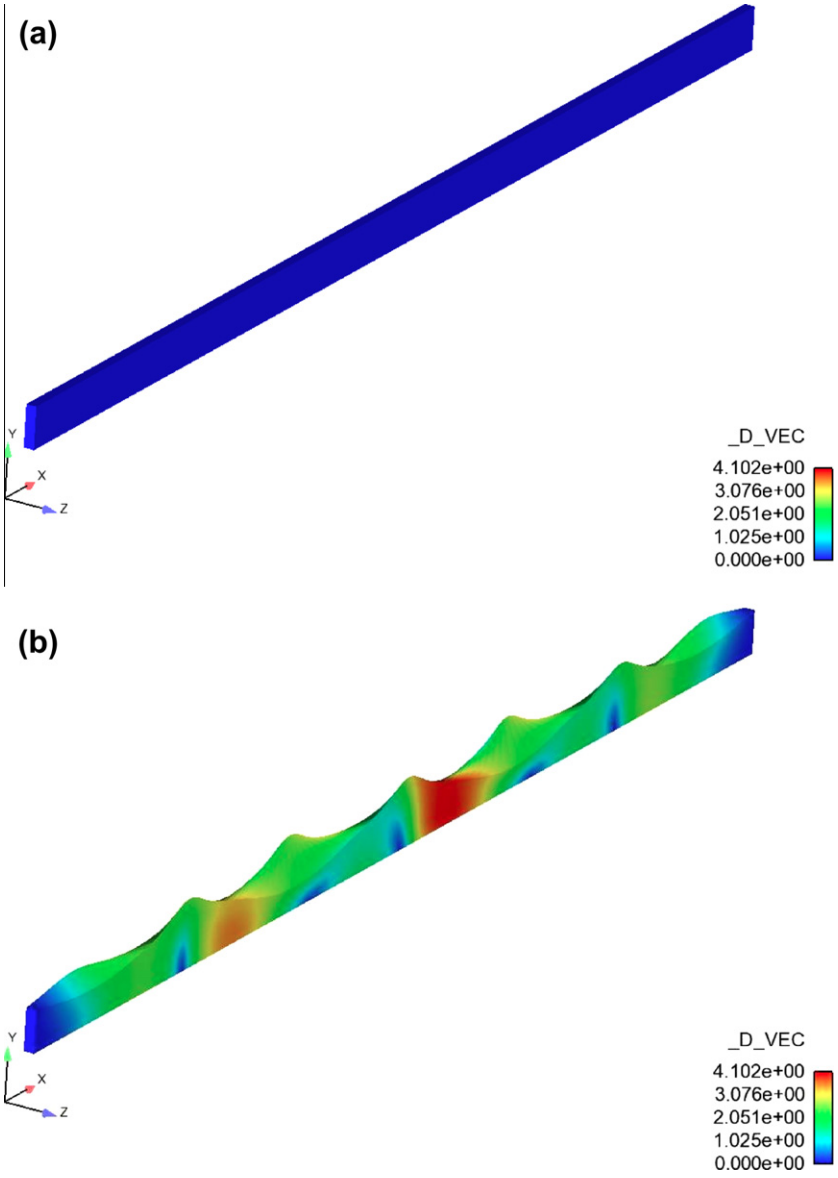

Fig. 7. 3D dielectric elastomer strip. (a) Undeformed strip; (b) illustration of wrinkling instability.

The deformation of the elastomer under potential loading is shown in Fig. 6; it is clear that the deformation history is significantly different than that under charge loading in Fig. 4. In particular, under potential loading, the elastomer undergoes the well-known pull-in instability when the maximum in the voltage-charge curve is reached whereby the elastomer expands rapidly in the planar directions, as shown in Figs. 6(b) and (c), while undergoing a corresponding reduction in film thickness. Specifically, the increase in film area in going from Fig. 6(a) to (c) is about 527%, while the corresponding reduction in film thickness is nearly 94%. Due to this enormous increase in film area and thus biaxial tensile strain shown in Fig. 6(c), the film is unstable under further potential loading, and a snap-back wrinkling instability is then observed, in Fig. 6(d), after which failure of the dielectric elastomer film occurs. This simulation makes clear that charge loading offers more flexibility in terms of enabling the elastomer to explore a significantly larger configurational space of deformations and thus possible actuation motions after the electromechanical instability has occurred.

5.3. Inhomogeneous deformation: wrinkling of a quasi-3D strip

Our final numerical example demonstrates the ability to capture localized electromechanical instabilities, such as wrinkling (Plante and Dubowsky, 2006). For this example, we considered a quasi-3D strip of dielectric elastomer with dimensions $120 \times 4 \times 1$; this geometry is similar to the "cuboid" geometry studied by Kofod (2008), and also the case of an elastomer attached to a rigid substrate, i.e. Wang et al. (2011). The strip was discretized with 480 8-node hexahedral finite elements with a regular element spacing of 1. The axial length of the strip was kept fixed in the x-direction, while the bottom $(-y)$ surface of the strip was fixed from moving in the y-direction. Finally, the strip was not allowed to deform in the z-direction. An electrode corresponding to zero applied voltage was applied to the bottom $(-y)$ surface of the strip while the electrostatic loading was applied through an applied voltage on the top $(+y)$ surface of the strip.

Fig. 7(a) shows the undeformed configuration, while Fig. 7(b) shows the wrinkled configuration of the elastomeric strip. The deformation history prior to wrinkling is interesting due to the fact that the wrinkling in Fig. 7(b) occurs almost immediately after a very small amount of compressive strain in the strip, on the order of <0.01%, is achieved. This suggests that a snap-through like path to the wrinkling instability is followed, where this hypothesis can be verified by analyzing the voltage vs. charge curve for the 3D elastomeric strip in Fig. 8. There, the wrinkling instability is detectable via the reduction in the slope of the voltage-charge curve, and thus a reduction in the film capacitance, at a normalized voltage of about 12. After formation of the wrinkles, the wrinkles are observed to propagate along the surface of the strip under further electrostatic loading. The remainder of the voltage-charge curve corresponds to the time history of the wrinkling instability, with eventual failure of the 3D strip at a normalized voltage near 16.

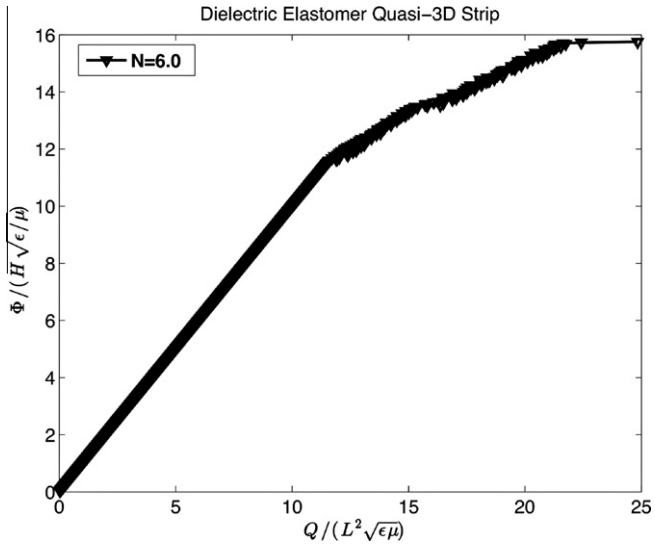

Fig. 8. Normalized voltage vs. charge curve for the quasi-3D wrinkling example shown in Fig. 7.

We also considered a quasi-3D strip with both active and passive regions, to conduct simulations similar in spirit to recent experimental studies (Pelrine et al., 2000; Plante and Dubowsky, 2006) in which the voltage was applied to only the (active) central region of the 3D strip, which was one half the total length of the strip, while two outer (passive) regions of the strip, each of which was one quarter the total length of the strip, were not subject to any applied electrostatic loading. This type of decomposition is typically performed experimentally to access the true material response of the dielectric elastomer by limiting the effects of stress concentrations that occur at the fixed ends of the dielectric elastomer. There were no kinematic constraints between the active and passive regions except the usual displacement continuity that is mandated and automatically enforced by the finite element approximation. Even for this case, we found that while the buckling instability initiated in the active region, it soon propagated to the passive region, thereby causing instability and buckling of the entire strip, similar to what is demonstrated in Fig. 7(b).

6. Conclusions

In conclusion, we have presented a nonlinear finite element formulation for the analysis of dielectric elastomers. We have demonstrated that by accounting for inertial effects in the governing mechanical equation of motion, inhomogeneous deformation modes, such as the pull-in instability and wrinkling, that result from electromechanical instabilities and that are the key factors in limiting the performance and reliability of dielectric elastomer transducers, can be captured and analyzed. Having demonstrated the robustness of the proposed finite element formulation, it is clear that it is suitable for future implementation in commercial finite element codes like ABAQUS or COMSOL to study electromechanical instabilities in dielectric elastomer transducers.

Acknowledgements

HSP acknowledges startup funding from Boston University in support of this research, and the assistance from Dr. Alejandro Mota with the Tahoe code. JZ acknowledges the support of NSFC through grants 10872157, 11072185, and 11021202. ZS acknowledges the support of ARO through contract W911NF-09-1-0476), DARPA through contract W911NF-10-1-0113, and MRSEC.

References

Arruda, E.M., Boyce, M.C., 1993. A three-dimensional constitutive model for the large stretch behavior of rubber elastic models. Journal of the Mechanics and Physics of Solids 41, 389–412.

Belytschko, T., Liu, W.K., Moran, B., 2002. Nonlinear Finite Elements for Continua and Structures. John Wiley and Sons.

Brochu, P., Pei, Q.B., 2010. Advances in dielectric elastomers for actuators and artificial muscles. Macromolecular Rapid Communications 31, 10–36.

Carpi, F., Bauer, S., De Rossi, D., 2010. Stretching dielectric elastomer performance. Science 330, 1759–1761.

Foo, C.C., Cai, S., Koh, S.J.A., Bauer, S., Suo, Z., 2012. Model of dissipative dielectric elastomers. Journal of Applied Physics 111, 034102.

Hong, W., 2011. Modeling viscoelastic dielectrics. Journal of the Mechanics and Physics of Solids 59, 637–650.
Huang, J., Li, T., Foo, C.C., Zhu, J., Clarke, D.R., Suo, Z., 2012. Giant, voltage-actuated deformation of a dielectric elastomer under dead load. Applied Physics Letters 100, 041911.
Hughes, T.J.R., 1987. The Finite Element Method: Linear Static and Dynamic Finite Element Analysis. Prentice-Hall.
Keplinger, C., Kaltenbrunner, M., Arnold, N., Bauer, S., 2008. Capacitive extensometry for transient strain analysis of dielectric elastomer actuators. Applied Physics Letters 92, 192903.
Keplinger, C., Li, T., Baumgartner, R., Suo, Z., Bauer, S., 2012. Harnessing snap-through instability in soft dielectrics to achieve giant voltage-triggered deformation. Soft Matter 8, 285–288.
Kofod, G., 2008. The static actuation of dielectric elastomer actuators: how does pre-stretch improve actuation? Journal of Physics D: Applied Physics 41, 215405.
Koh, S.J.A., Li, T., Zhou, J., Zhao, X., Hong, W., Zhu, J., Suo, Z., 2011. Mechanisms of large actuation strain in dielectric elastomers. Journal of Polymer Science Part B: Polymer Physics 49, 504–515.
Kollosche, M., Kofod, G., 2010. Electrical failure in blends of chemically identical, soft thermoplastic elastomers with different elastic stiffness. Applied Physics Letters 96, 071904.
Norris, A.N., 2008. Comment on "Method to analyze electromechanical stability of dielectric elastomers" [Applied Physics Letters 91, 061921 (2007)]. Applied Physics Letters 92, 026101.
O'Brien, B., McKay, T., Calius, E., Xie, S., Anderson, I., 2009. Finite element modelling of dielectric elastomer minimum energy structures. Applied Physics A: Materials Science and Processing 94, 507–514.
Pelrine, R., Kornbluh, R., Pei, Q., Joseph, J., 2000. High-speed electrically actuated elastomers with strain greater than 100%. Science 287, 836–839.
Plante, J.-S., Dubowsky, S., 2006. Large-scale failure modes of dielectric elastomer actuators. International Journal of Solids and Structures 43, 7727–7751.
Suo, Z., Zhao, X., Greene, W.H., 2008. A nonlinear field theory of deformable dielectrics. Journal of the Mechanics and Physics of Solids 56, 467–486.
Suo, Z., 2010. Theory of dielectric elastomers. Acta Mechanica Solida Sinica 23, 549–578.
Tahoe, 2011. Available at: <http://sourceforge.net/projects/tahoe/>.
Vu, D.K., Steinmann, P., Possart, G., 2007. Numerical modelling of non-linear electroelasticity. International Journal for Numerical Methods in Engineering 70, 685–704.
Wang, Q., Zhang, L., Zhao, X., 2011. Creasing to cratering instability in polymers under ultrahigh electric fields. Physical Review Letters 106, 118301.
Wissler, M., Mazza, E., 2005a. Modeling of a pre-strained circular actuator made of dielectric elastomers. Sensors and Actuators A 120, 184–192.
Wissler, M., Mazza, E., 2005b. Modeling and simulation of dielectric elastomer actuators. Smart Materials and Structures 14, 1396–1402.
Wissler, M., Mazza, E., 2007. Mechanical behavior of an acrylic elastomer used in dielectric elastomer actuators. Sensors and Actuators A 134, 494–504.
Zhao, X., Hong, W., Suo, Z., 2007. Electromechanical hysteresis and coexistent states in dielectric elastomers. Physical Review B 76, 134113.
Zhao, X., Suo, Z., 2007. Method to analyze electromechanical stability of dielectric elastomers. Applied Physics Letters 91, 061921.
Zhao, X., Suo, Z., 2008. Method to analyze programmable deformation of dielectric elastomer layers. Applied Physics Letters 93, 251902.
Zhao, X., Suo, Z., 2010. Theory of dielectric elastomers capable of giant deformation of actuators. Physical Review Letters 104, 178302.
Zhou, J., Hong, W., Zhao, X., Zhang, Z., Suo, Z., 2008. Propagation of instability in dielectric elastomers. International Journal of Solids and Structures 45, 3739–3750.